Scientific Reports

https://doi.org/10.1038/s41598-026-61304-0

Article in Press

Artificial neural network modeling to predict corrective stress of a two-layer composite plate under fully reversed cyclic loading using the finite element method & morrow method

Received: 27 March 2026

Accepted: 3 July 2026

Published online: 07 July 2026

Cite this article as: Alkhafaji A., Khalaf M.I., Kh. T.I. *et al.* Artificial neural network modeling to predict corrective stress of a two-layer composite plate under fully reversed cyclic loading using the finite element method & morrow method. *Sci Rep* (2026). https://doi.org/10.1038/s41598-026-61304-0

Ali Alkhafaji, Mohammed I. Khalaf, Teeba Ismail Kh., Narinderjit Sawaran SinghSingh, Shaymaa Abed Hussein, Mahmood Alsaadi, Dheyaa J. Jasim, Mahmut Taner & Soheil Salahshour

Artificial Neural Network Modeling to Predict Corrective Stress of a Two-layer Composite Plate under Fully Reversed Cyclic Loading Using the Finite Element Method & Morrow Method

1. Ali Alkhafaji

Advanced Technical College, University of Warith Al-Anbiyaa, Karbala, Iraq
ali.basim.alkhafagi@uowa.edu.iq

2. Mohammed I. Khalaf
Department of Computer Sciences, College of Science, University of Al Maarif, Al Anbar,31001, Iraq
m.i.khalaf@uoa.edu.iq

3. Teeba Ismail Kh.
Department of Computer Engineering, College of Engineering and Computer Science, Lebanese French University, Erbil, Kurdistan Region,Iraq
teeba.ismail@lfu.edu.krd

https://orcid.org/0000-0001-5792-9548

4. Narinderjit Singh Sawaran Singh
Faculty of Data Science and Information Technology, INTI International University, Persiaran Perdana BBN, Putra Nilai, Nilai 71800, Malaysia.
narinderjits.sawaran@newinti.edu

5. Shaymaa Abed Hussein
Department of Pathological Analyzes, Al Manara College for Medical Sciences, Maysan, Iraq.

6. Mohmood Alsaadi

Department of Computer Sciences, College of Science, University of Al Maarif, Al Anbar,31001, Iraq
Alsaadi.m@uoa.edu.iq

7. Dheyaa J. Jasim

College of Engineering, University of Al Maarif, Al Anbar,31001, Iraq.
dheyaa.jumaah@uoa.edu.iq

8- Mahmut Taner

Istanbul Gelisim University, Department of Web Design and Development, 34310, Istanbul, Turkiye.

9- Soheil Salahshour*

Faculty of Engineering and Natural Sciences, Istanbul Okan University, Istanbul, Turkey
Faculty of Engineering and Natural Sciences, Bahcesehir University, Istanbul, Turkey
Research Center of Applied Mathematics, Khazar University, Baku, Azerbaijan

Faculty of Science and Letters, Piri Reis University, Tuzla, Istanbul, Turkey

soheil.salahshour1361@gmail.com

***Corresponding Author:** Soheil Salahshour; soheil.salahshour1361@gmail.com

Abstract

In this study, a single-hidden-layer feedforward Artificial Neural Network was developed to predict the maximum stress of a two-layer composite plate based on the Morrow correction method under fully reversed cyclic loading. A rectangular two-layer plate made of Epoxy Carbon Woven (230 GPa) was analyzed using the Finite Element Method for various fiber orientations of each layer (0°, 15°, 30°, 45°, 60°, 75°, and 90°) relative to the transverse axis. The results indicate that a 0° fiber orientation in both layers produced the maximum stress, potentially weakening the plate under tensile load, whereas a 90° orientation minimized stress and enhanced tensile strength. Increasing the second-layer angle while keeping the first layer fixed reduced stress, whereas decreasing the first-layer angle for a fixed second-layer angle increases stress. Maximum stress regions shifted from localized points to linear distributions, sometimes moving from uniform edge distributions to mid-edge concentrations. When both layers had identical angles, the stress magnitude increased, and the maximum stress shifted from the loaded edge to a corner, indicating stress concentration and a potential reduction in lifespan. The Artificial Neural Network demonstrated excellent predictive performance, achieving an optimal validation Mean Squared Error of 3.2266×10^{-4} at iteration 22, with a minimum overall Mean Squared Error of 6.5566×10^{-4} across all datasets. The correlation coefficients for the training, validation, test, and entire datasets were 0.99508, 0.98649, 0.99484, and 0.99485, respectively, indicating a strong agreement between the Mean Squared Error predictions and Finite Element Method-simulated values.

Keywords: Composite Sheet, Fiber Angle, Corrective Stress, Finite Element Method, Morrow Method, Artificial Neural Network

Abbreviation

Artificial Neural Network	ANN
Levenberg–Marquardt	LM
Mean squared error	MSE
Correlation coefficients	R
Finite Element	FE

1. Introduction

In recent decades, composite materials have been increasingly recognized as advanced alternatives to conventional metallic materials in various engineering fields [1]. Their unique characteristics, including a high strength-to-weight ratio, superior resistance to corrosion and fatigue, and the ability to tailor structural performance through laminate design, have made them indispensable in modern industries such as aerospace, automotive, marine engineering, wind energy, and biomedical applications [2, 3]. Among various categories of fiber-reinforced composites, carbon fiber-reinforced polymers (CFRPs) garnered particular attention. Within this category, laminated composite plates are widely used due to their design flexibility and superior mechanical properties[4]. The fiber orientation in each ply can be strategically selected to optimize the laminate's global stiffness and strength under specific loading conditions. As a result, fiber orientation plays a crucial role in identifying the stress distribution, deformation characteristics, and fatigue performance of composite laminates [5, 6]. A significant concern in the application of laminated composites is their fatigue performance under cyclic loading[7]. Unlike static failure, which typically occurs at relatively high stress levels, fatigue damage can initiate at significantly lower stress amplitudes and propagate over time, often becoming the dominant failure mode under service conditions [8]. Moreover, fatigue failure typically occurs before the ultimate static strength is reached, thereby limiting the reliability and durability of structural components [9]. To enhance the accuracy of fatigue life prediction, several models have been developed to incorporate the influence of mean stress[10]. Among these, the Morrow mean stress correction model is one of the most widely employed approaches. By accounting for mean stress effects by modifying the effective stress amplitude, the Morrow model enables more reliable estimation of the maximum (Max) effective stresses contributing to fatigue damage, especially under alternating tensile and compressive loading [11]. Wei et al.[12] developed an efficient methodology to characterize the out-of-plane shear behavior of thick-section fiber-reinforced polymer composites. By integrating a plate torsion test with an artificial neural network (ANN) trained on three-dimensional finite element (FE) simulations and digital image correlation (DIC), they accurately predicted the nonlinear shear stress–strain response. The approach enabled the iterative extraction of constitutive parameters for a 15-ply glass/epoxy panel with high precision (average error <0.5%) and improved stress-update efficiency by a factor of 10. Liu et al. [13] proposed a novel methodology to predict local elastic properties of unidirectional polymeric composite plates by combining the Impulse Excitation Technique (IET) with machine learning (ML). The framework employed fiber volume fraction and plate thickness as input parameters, using the first resonance frequencies at multiple fiber orientations to accurately represent the composites' anisotropic characteristics.The findings indicated that the deep neural network (DNN) model achieved highly reliable predictions, with R^2 values exceeding 0.9 in both the training and test datasets, demonstrating strong performance in estimating Young's moduli. Marković et al. [14] developed a surrogate ANN model to efficiently predict the fatigue life of steel components with stress concentrators. Trained on data from a parametrized FE-based model, the ANN accurately generates component-specific S-N curves for both through- and surface-hardened steels. While the FE model provides detailed, nonlinear stress–strain responses at high computational cost, the ANN offers a faster, more reliable alternative for fatigue life assessment across varying geometries and heat-treatment conditions. Despite the advances in numerical modeling, accurately predicting the fatigue-related stress behavior of laminated composites under fully reversed cyclic loading remains a significant challenge due to the inherent complexity of their mechanical response. The interactions among ply properties, fiber orientation, stacking sequence, boundary conditions, and loading configurations result in highly nonlinear, multivariate behavior that is difficult to capture efficiently with conventional analytical or high-fidelity numerical methods. Although FE method simulations can provide detailed insights into stress distributions and fatigue performance, their computational cost and time requirements limit their practical application, particularly for parametric studies and design optimization[15].To address these limitations, ANNs have emerged as a powerful alternative, capable of efficiently capturing complex, nonlinear, and multivariate mechanical behaviors without requiring explicit constitutive formulations. By training on high-fidelity datasets generated from FE method simulations and experimental measurements, ANNs serve as surrogate models that provide accurate predictions while significantly reducing computational cost and time [16]. In the present study, an ANN-based framework was developed to predict the corrective stress of a two-layer composite plate under fully reversed cyclic loading. The model leveraged FE simulations in combination with the Marrow method to generate data, enabling systematic iterative network training and validation. This integrated approach not only allowed for rapid and reliable evaluation of fatigue-sensitive stress behavior and cyclic stress redistribution but also facilitated the extraction of critical material parameters and stress responses under complex loading conditions. Consequently, the proposed methodology provided a versatile and scalable tool for the design, optimization, and performance assessment of laminated composite structures, bridging the gap between high-fidelity numerical modeling and practical engineering applications.

2. Methodology

2.1. Morrow tension corrector method

To determine the stresses induced by cyclic loading on a structure, the static response under the applied loads must first be analyzed. The resulting stress-strain distributions were then evaluated under fatigue conditions to obtain the corresponding cyclic stresses and strains. Subsequently, the strain tensor history was determined as a function of time, based on the type and characteristics of the applied loading. In most cases, the strains at this stage were linearly elastic. One of the key factors influencing the magnitude of cyclic stresses was the waveform of the applied load. Fully reversed cyclic loading with constant amplitude was a common fatigue load used in such analyses. To incorporate these cyclic loads into fatigue assessments, the linear superposition method was employed, in which the weighted static stress results are combined to determine the two-point cyclic stress according to the specified equation (Eq. 1).

$$\begin{aligned}&\text{First Point:}\sigma_{ij}=\sum_k(\text{Max Factor})_k.\sigma_{ij,k.static}\\&\text{Second Point:}\sigma_{ij}=\sum_k(\text{Min Factor})_k.\sigma_{ij,k.static}\end{aligned}\tag{1}$$

<u>In Eq.1, k represents the summation index associated with the loading steps used in the cyclic stress superposition procedure.</u> Using a unit load factor with the default maximum (Max) and minimum (Min) coefficients (1 and –1, respectively) resulted in a fully reversed cyclic loading simulation with a constant amplitude. Based on the type of cyclic load, the local strain was used to derive the corresponding cyclic stress-strain response and to predict the shape of the resulting hysteresis loops. In this study, the uniaxial cyclic stress-strain behavior was modeled using the Ramberg-Osgood relationship, as expressed in Eq.2 [17].

$$\varepsilon_a=\frac{\sigma_a}{E}+\left(\frac{\sigma_a}{K}\right)^{\frac{1}{n}}\tag{2}$$

To predict the shape of each hysteresis loop, the cyclic stress-strain curve can be doubled in magnitude according to Masing's hypothesis, as expressed in Eq. 3.

$$\Delta\varepsilon=\frac{\Delta\sigma}{E}+2\left(\frac{\Delta\sigma}{2K}\right)^{\frac{1}{n}}\tag{3}$$

In the above equation, ε represents the strain, σ the stress, E the Young's modulus, and n and k are material-dependent constants. The nonlinear cyclic stress–strain behavior of Epoxy Carbon Woven composite material was characterized using the Ramberg–Osgood constitutive relationship within the ANSYS strain-life fatigue analysis framework. In the present FE model, the strain-hardening exponent (n) was set to 1.8, and the strength coefficient (K) was set to 77 MPa. When it is necessary to account for errors arising from cyclic strain in the stress-strain relationship, and if the standard error of the logarithm of cyclic strain (SEc) exceeds 1, the cyclic stress-strain behavior can be determined using Eq.4.

$$\Delta\varepsilon = \frac{\Delta\sigma}{E} + 2\left(\frac{2\sigma}{2K'}\right)^{\frac{1}{n'}} .10^{\text{-z.SEc}} \tag{4}$$

In the present study, the Smith–Watson–Topper (SWT) method was employed, assuming zero cyclic-strain error. Using the elastic strain tensor, a combined strain parameter was determined. In the current analysis, the absolute Maximum principal strain was selected as the governing strain criterion because laminated composite materials exhibit highly anisotropic mechanical behavior, leading to simultaneous longitudinal and transverse strain development under cyclic loading. This parameter provides an effective representation of the local multiaxial deformation state and enables the reliable identification of fatigue-sensitive regions within the composite laminate. Therefore, considering the combined strain response was essential for accurately predicting fatigue behavior and avoiding significant errors associated with simplified uniaxial strain assumptions. The combined strain history was then analyzed using the rainflow counting method to extract a list of load cycles, while simultaneously estimating the local total elastic-plastic strain according to Neuber's rule and determining the shape and position of each hysteresis loop. The local strain approach required defining the total elastic-plastic strain range for each cycle, and it often necessitated the corresponding mean or Max stress. Fatigue damage was then calculated using Miner's rule and the material-specific E-N curve. Stress-correction methods enabled incorporating the effects of mean stress or multiaxial loading into fatigue-life predictions. One common approach was the Morrow correction, widely used in composite structures to account for the influence of mean stress under cyclic loading. The present study considered fully reversed cyclic loading conditions (R=-1), for which the mean stress was theoretically zero. Under such conditions, the classical strain-life formulation and the Morrow-corrected formulation yielded nearly identical results.

Nevertheless, the Morrow correction framework was retained in the present analysis to establish a generalized fatigue modeling procedure that can be readily extended to cyclic loading cases involving non-zero mean stress conditions in future investigations. Fatigue calculations based on FE analysis are typically derived from elastic results, so the equivalent strain obtained from strain-life analysis showed pseudo-elastic behavior depending on the type of loading. In multiaxial stress states, rainflow counting should be combined with the Neuber or Hoffman-Sieger methods to accurately estimate the total strain range for each cycle and accurately capture the resulting hysteresis loops. It is essential to consider that composite materials are heterogeneous and anisotropic, unlike metallic structures. This means that their mechanical properties varied along different directions of the constituent plies. Furthermore, properties such as static strength and fatigue resistance were highly dependent on the alignment of applied load with respect to the fiber orientation, underscoring the need to account for material anisotropy in any analysis of composite structures.

2.2. FE Modeling

The composite plate model analyzed in this study consisted of two layers of epoxy carbon woven material with a Young's modulus of 230 GPa. The plate had a total thickness of 10 mm and in-plane dimensions of 500 by 500 mm. One edge of the plate was fully constrained to simulate a fixed support. In contrast, a cyclic load of 100,000 N with constant amplitude and fully reversed characteristics was applied along the opposite edge, as illustrated in Fig.1. This configuration allowed for the investigation of the plate's response under fully reversed cyclic loading. It facilitated the analysis of stress redistribution, strain response, and fatigue-related stress behavior across the composite layers.

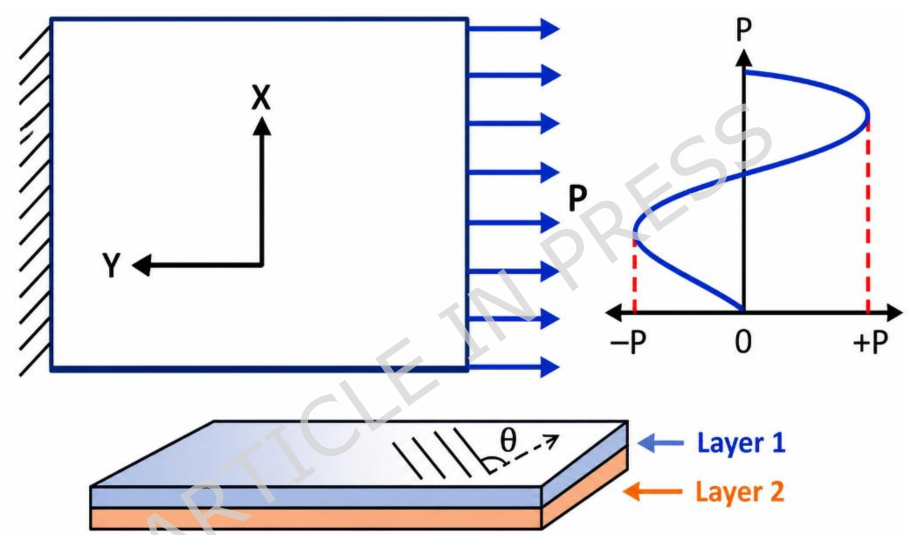

Fig.1: Model geometry under oscillating load P, along with layer arrangement schematic.

FE analysis was conducted using ANSYS to investigate the mechanical response of a two-layer epoxy carbon woven composite plate. The plate was modeled with one edge fully constrained. In contrast, a constant load was applied at the opposite edge, as shown in Fig. 1. Cyclic loading conditions were subsequently defined for a strain-life analysis, and the Morrow stress correction method was used to account for mean stress effects. In the present FE framework, material nonlinearity associated with cyclic elastic-plastic stress–strain behavior was considered through the strain-life fatigue analysis combined with the Morrow mean stress correction and Neuber-based stress correction procedures. Nevertheless, the model did not include an explicit progressive damage evolution formulation, such as stiffness degradation, delamination growth, or continuum damage mechanics. Therefore, the present analysis primarily focused on the corrected cyclic stress response and fatigue-related stress redistribution behavior of the laminated composite plate under fully reversed loading conditions. The resulting strains were calculated, and the corresponding stresses were obtained from cyclic stress-strain relationships. The mechanical properties and strain limits of the epoxy carbon woven (230 GPa) wet composite material used in the present FE simulations are summarized in Tables 1 and 2, respectively. Table 1 presents the orthotropic elastic and strength properties of the composite material, including Young's moduli, Poisson's ratios, shear moduli, and tensile/compressive strength parameters in different material directions. These properties were used to accurately represent the anisotropic mechanical behavior of the laminated composite under cyclic loading.

Table 1: Elasticity properties of Epoxy Carbon Woven (230 GPa) Wet material**.**

Orthotropic Elasticity	
Young's Modulus X direction (MPa)	61340
Young's Modulus Y direction (MPa)	61340
Young's Modulus Z direction (MPa)	6900
Poisson's Ratio XY	0.04
Poisson's Ratio YZ	0.3
Poisson's Ratio XZ	0.3
Shear Modulus XY (MPa)	19500
Shear Modulus YZ (MPa)	2700
Shear Modulus XZ (MPa)	2700
Tensile Strength X direction (MPa)	805
Tensile Strength Y direction (MPa)	805
Tensile Strength Z direction (MPa)	50
Compressive Strength X direction (MPa)	-509
Compressive Strength Y direction (MPa)	-509
Compressive Strength Z direction (MPa)	-170

Table 2 presents the corresponding tensile, compressive, and shear strain limits used in the strain-life fatigue analysis. These parameters defined the allowable deformation thresholds under cyclic loading conditions and served as essential input data for the FE-based fatigue simulations and stress-correction procedures employed in the present study.

Table 2: Tensile, compressive, and shear strain limits of Epoxy Carbon Woven (230 GPa) Wet material

Orthotropic Strain Limit	
Tensile X direction	0.012
Tensile Y direction	0.012
Tensile Z direction	0.012
Compressive X direction	-0.01
Compressive Y direction	-0.01
Compressive Z direction	-0.01
Shear XY	0.019
Shear YZ	0.014
Shear XZ	0.019

The FE model of the laminated composite plate was discretized using two-dimensional quadrilateral FEs. These elements were selected for their ability to accurately represent stress gradients and deformation behavior in layered composite structures subjected to cyclic loading. Following the mesh convergence analysis, the final mesh configuration was selected to ensure an appropriate balance between numerical accuracy and computational efficiency. The resulting FE mesh used in the present simulations is illustrated in Fig. 2.

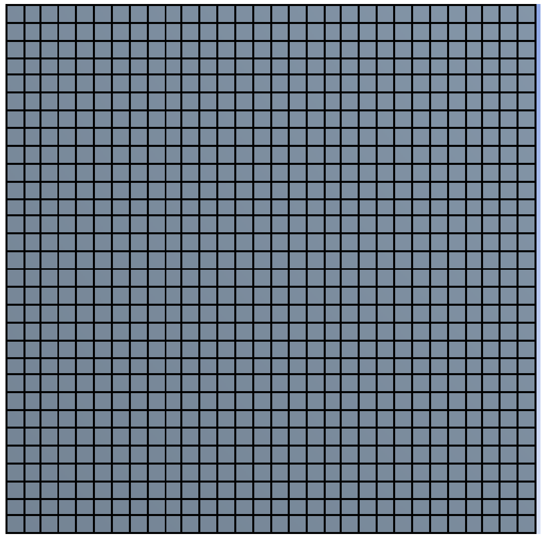

Fig.2. FE model of composite sheet.

To ensure numerical reliability and accuracy in FE simulations, a mesh-convergence analysis was conducted before the main calculations. The convergence study was conducted for the representative case in which both composite plies were oriented at 90∘. Several mesh densities with different numbers of FEs were examined, and the corresponding Max stress values were monitored, as illustrated in Fig. 3. The obtained results demonstrate that the predicted stress values gradually converged with increasing mesh density, while the variation in Max stress became negligible for finer meshes. The difference between the final two mesh refinements was found to be very small, indicating that the numerical solution became effectively mesh-independent. Therefore, the selected mesh configuration provided an appropriate balance between computational accuracy and numerical efficiency, ensuring the credibility and stability of the generated stress contour distributions and FE results.

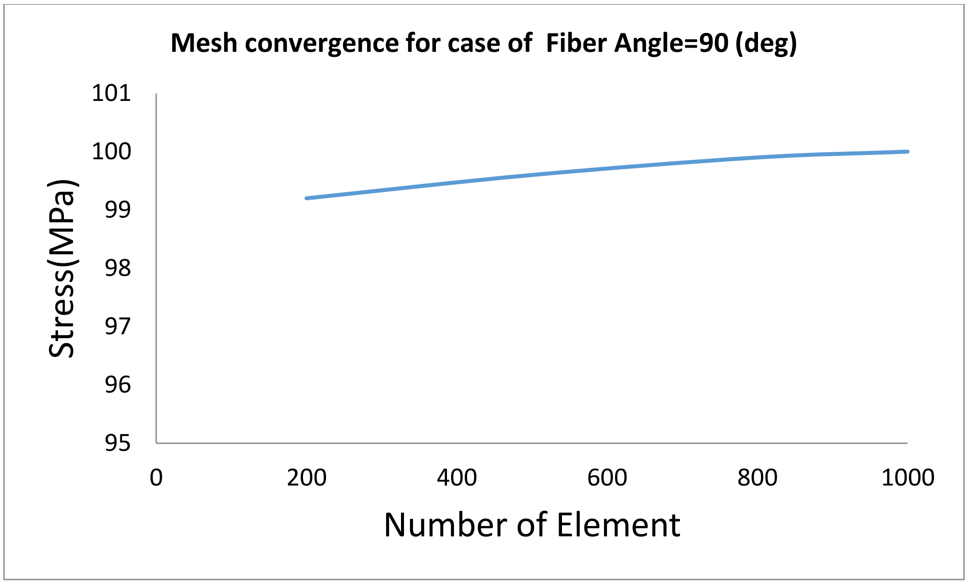

Fig. 3. Mesh convergence analysis for the composite plate with 90∘ fiber orientation in both layers.

The analysis began with determining the elastic strain history, which was combined with the cyclic stress-strain curve and Neuber's rule to estimate local elastic-plastic stresses and strains. Residual strain loops were then incorporated with the Neuber correction to determine the response for successive cycles. In the present study, Neuber's rule was implemented within the FE-based strain-life analysis framework to estimate the local elastic-plastic stress–strain response from the initially obtained elastic FE results. The Neuber correction was further applied during the evaluation of residual-strain hysteresis loops under fully reversed cyclic loading conditions to account for local plasticity effects and cyclic stress redistribution. It should be noted that the ANN model did not implement Neuber's rule directly. Instead, the ANN was trained on the final stress dataset generated from the FE simulations, after applying the Morrow correction method and the Neuber-based elastic-plastic stress correction procedure. This procedure was iteratively applied across all cycles to obtain the mean and maximum stress for each cycle, completing the full strain history. The study considered 49 different ply configurations with fiber orientations relative to the X-axis, as illustrated in Fig. 1. The Maximum stress values for each fiber orientation configuration are presented in Table 3. Results indicate that a 0° fiber orientation in both layers produced the highest stresses, increasing the plies' susceptibility to tensile loads perpendicular to the fiber direction. Conversely, a 90° fiber orientation produced the lowest stresses, enhancing the plate's resistance to tensile loads applied along the fiber direction. These findings highlighted the significant impact of fiber orientation on stress distribution and overall mechanical performance in laminated composite plates.

Table 3. Max stress values corresponding to different fiber orientation configurations.

Angle 1 (deg)	**Angle 2 (deg)**	**Stress(Mpa)**
0	0	262
0	15	250
0	30	240
0	45	210
0	60	198
0	75	190
0	90	154
15	0	242
15	15	232
15	30	228
15	45	200
15	60	180
15	75	160
15	90	145
30	0	232
30	15	204
30	30	190
30	45	180
30	60	175
30	75	150
30	90	133
45	0	220
45	15	203
45	30	185
45	45	175
45	60	166
45	75	145
45	90	130
60	0	222
60	15	204
60	30	198
60	45	172
60	60	157
60	75	130
60	90	121
75	0	197

75	15	185
75	30	175
75	45	166
75	60	130
75	75	121
75	90	105
90	0	173
90	15	166
90	30	150
90	45	140
90	60	110
90	75	105
90	90	100

Fig. 4 illustrates the variation in the maximum stress in the composite as a function of the fiber orientation angle in the second ply, plotted separately for each selected orientation of the first ply fibers. As observed in Fig.4, an increase in the fiber angle of the second ply, for any fixed orientation of the first ply, results in a reduction of the applied stress. Conversely, for any fixed orientation of the second ply, decreasing the fiber angle of the first ply led to an increase in the resulting stress. As expected, the composite's highest strength corresponded to the configuration in which both plies were aligned at 90°, since in this case the fiber directions were fully aligned with the applied load, thereby maximizing load-bearing capacity.

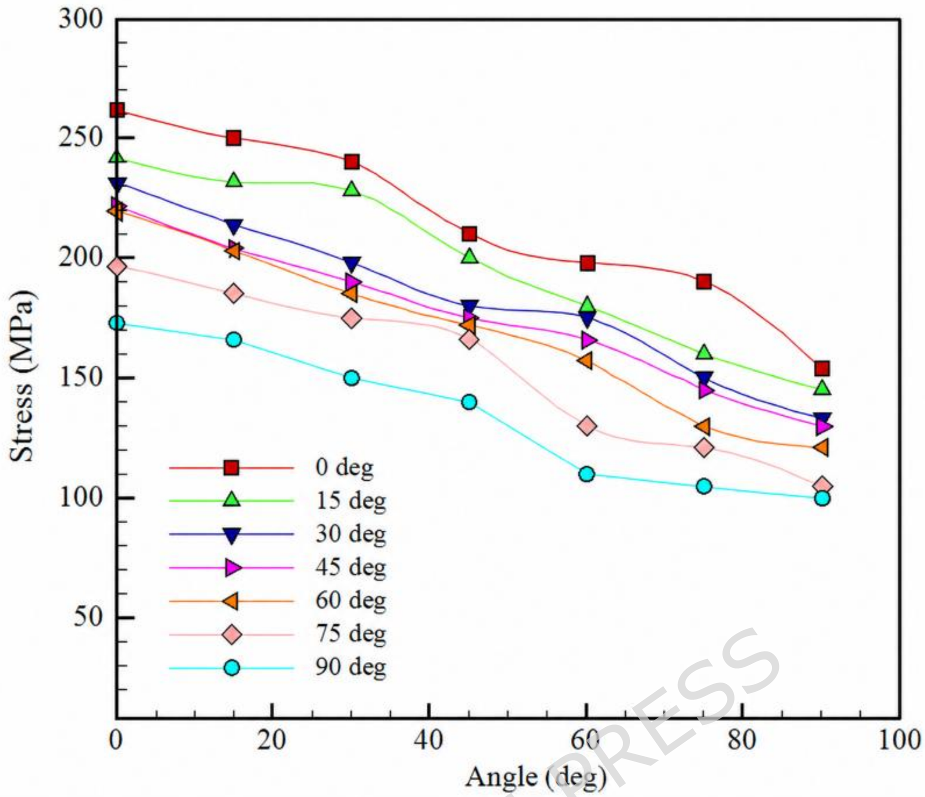

Fig.4: Max stress behavior for each of the fiber arrangement states of layers.

Fig.5 presents the stress contour distribution over the studied composite plate under the considered configuration. By comparing the stress contours corresponding to cases where the fiber angle of the first ply was fixed and the angle of the second ply increased, it can be observed that, in addition to the overall reduction in stress magnitude, the regions of Max stress transition from localized point-like zones to extended line-shaped regions. In some cases, the distribution of peak stresses also changed from being relatively uniform along the plate edge to becoming concentrated at the mid-edge. Furthermore, results for configurations in which both plies were oriented at identical fiber angles, compared with those in which the ply orientations differ, indicate not only an increase in stress but also a shift in the location of Max stress from the loaded edge toward the lower corner of the plate. This shift showed the concentration of stresses in localized regions, which, in turn, implied reduced fatigue life and structural durability of the composite plate. Moreover, increasing the fiber orientation angle of the second ply to 90∘ resulted in a noticeable reduction in the predicted maximum stress. This behavior can be attributed to stress redistribution resulting from changes in the laminate's anisotropic stiffness. At higher fiber orientation angles, the load transfer mechanism within the composite structure became more uniformly distributed, reducing localized stress concentrations near the loaded regions. In addition, the altered fiber alignment altered the laminate's directional resistance to deformation, thereby improving stress dissipation throughout the plate. Consequently, the stress field became smoother and less concentrated, which contributed to enhanced structural resistance and potentially improved fatigue durability of the composite system.

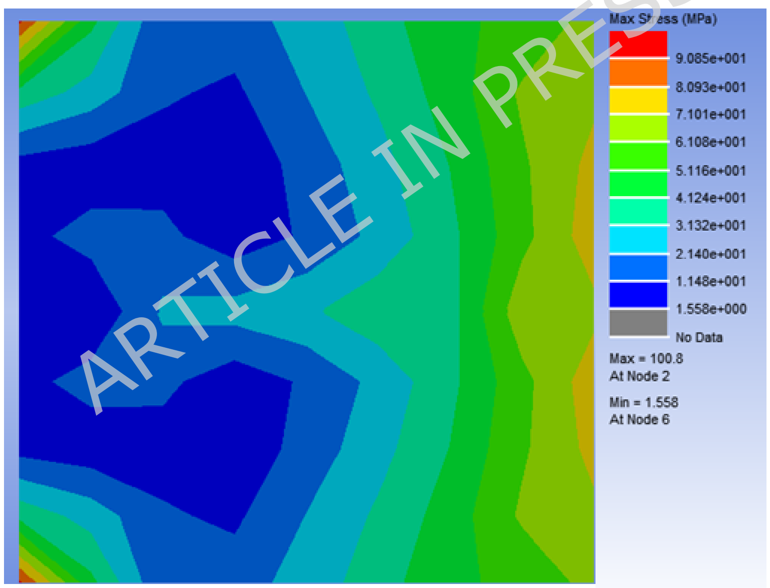

Fig.5: Stress contour for 90° fiber angles in each of the two layers of the composite sheet.

3. ANN Structure and Modeling

A feedforward ANN was employed to develop a predictive model for estimating the maximum stress in a composite plate. Feedforward NNs are one of the two principal categories of ANNs, which were characterized by unidirectional information propagation across their layers [18]. Unlike recurrent NNs, which relied on cyclic connections and feedback loops, feedforward networks transfer data sequentially from the input layer through the hidden layers (if present) to the output layer. Due to their simple yet robust structure, these networks were widely adopted for supervised learning tasks, which were commonly trained using the backpropagation algorithm [27-29, 19]. In the present research, a two-layer feedforward ANN was designed and implemented in MATLAB [18]. The network architecture consisted of a single hidden layer with five neurons, as depicted schematically in Fig. 6. The number of hidden neurons was determined through a comparative trial-and-error procedure involving several ANN architectures with different hidden neuron counts. The performance of each configuration was evaluated based on the Mean Squared Error (MSE), regression accuracy, and generalization capability. Networks with fewer neurons exhibited insufficient learning capability, whereas larger network structures increased the possibility of overfitting due to the limited dataset size. Among the examined architectures, the ANN model with 5 hidden neurons provided the best balance between prediction accuracy, computational efficiency, and model robustness.

The reliability of the selected architecture was further confirmed using K-fold cross-validation and coefficient of variation (CV) analysis. This model aimed to establish a reliable mapping between the input variables, namely the fiber orientation angles of two plies, and the output response, which corresponded to the Max stress in the composite plate. To generate the training and validation datasets, 49 data samples were obtained from FE simulations. The FE-generated dataset used as input for ANN training was obtained from strain-life analyses incorporating the Morrow mean stress correction method. Therefore, the target stress values employed in the ANN model correspond to Morrow-corrected stresses rather than purely elastic FE stress results. These data were systematically divided into three subsets: 70% for training, 15% for validation, and 15% for testing, thereby ensuring an unbiased assessment of the network's generalization performance. The learning process was carried out using the Levenberg–Marquardt (LM) optimization algorithm, which used error backpropagation to update the weight and bias parameters iteratively. To evaluate the model's predictive accuracy, the MSE between the network outputs and the target values was used as the performance index. The results confirmed that the proposed ANN architecture can accurately capture the nonlinear relationship between fiber orientation and maximum stress. Consequently, the developed model can be regarded as a powerful computational tool for analyzing and optimizing fiber-reinforced composite structures, offering both efficiency and reliability compared to conventional numerical methods.

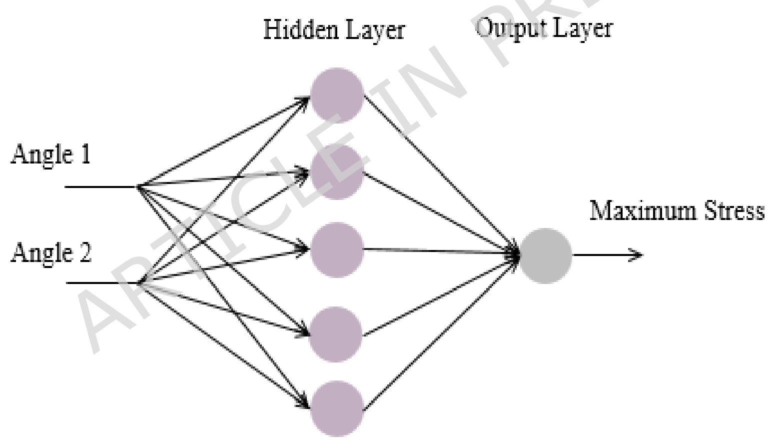

Fig. 6: A two-layer backpropagation NN for stress prediction.

3.1.LM optimization algorithm

The LM optimization algorithm, as described in Numerical Optimization by Nocedal and Wright, was employed to update and fine-tune the network parameters, including weights and biases, during the training process[20, 21]. The LM algorithm was particularly well-suited for problems where the loss performance was defined as a sum of squared errors, making it highly efficient for training feedforward NNs. Unlike second-order methods that require the explicit computation of the Hessian matrix, the LM algorithm approximates the Hessian by exploiting the Jacobian matrix J of the network errors with respect to the parameters. This approach combined the advantages of the gradient descent method and the Gauss–Newton algorithm, achieving faster convergence while maintaining numerical stability. Considering a loss performance f defined as the sum of squared errors e, it can be expressed as follows:

$$f = \sum_{i=1}^{m} e_i^2 \tag{5}$$

Here, m denotes the total number of training samples used in the learning process. In the context of the LM algorithm, the Jacobian matrix of the loss performance is particularly important, as it captures the sensitivity of the network's errors to its parameters. More precisely, the Jacobian is the matrix whose entries are the partial derivatives of the individual error terms with respect to the NN's adjustable weights (and biases). Each row of the Jacobian corresponded to a training sample, while each column corresponded to a specific network parameter. Consequently, the Jacobian encapsulates how slight variations in the parameters influenced the overall error distribution across all samples. This formulation not only facilitated the efficient approximation of the Hessian matrix but also enabled rapid convergence of the optimization process, a key strength of the LM method [22].

$$J_{i,j} = \frac{\partial e_i}{\partial w_j} \tag{6}$$

Let i=1,…,m denote the index over all training samples and j=1,…,p denote the index over all trainable parameters of the ANN, where p represents the total number of adjustable weights and biases. Under this formulation, the gradient vector of the loss function can be systematically computed by summing the gradients of its components, indicating the rate of change of the loss function with respect to each parameter and thereby quantifying the loss function's sensitivity to that parameter. This information is essential for optimization algorithms, as it guides the parameter updates required to minimize the difference between predicted and target outputs. In other words, by iteratively adjusting the parameters in the direction opposite the gradient, the model can progressively reduce its error and improve predictive accuracy. The mathematical expression for the gradient vector of the loss function is given as follows [23].

$$\nabla f = 2J^T.e \tag{7}$$

In the LM optimization approach, the vector e collects all individual error terms, representing the differences between the predicted outputs and their corresponding targets for the entire training dataset. Direct computation of the Hessian matrix H, which involved second-order derivatives of the loss function with respect to network parameters, was computationally intensive and often impractical for large networks. To overcome this limitation, the Hessian is approximated using the Jacobian matrix J, which contains the first-order derivatives of the errors with respect to the adjustable weights and biases. This approximation leveraged the inherent structure of squared-error loss, enabling the optimization algorithm to update parameters while maintaining efficient convergence. By using J instead of the full Hessian, the LM algorithm strikes a balance between computational cost and training performance, ensuring stable and effective learning in NNs. The Hessian matrix can thus be expressed approximately as a function of the Jacobian, as shown in the following formulation[24].

$$H \approx 2J^T.J + \lambda I \tag{8}$$

To ensure the Hessian approximation remains positive definite during NN training, the LM algorithm introduces a damping factor, λ. This factor is particularly important when the Jacobian matrix is poorly conditioned or when the current solution lies far from the Min of the loss function. By combining the damping factor with the identity matrix I, the algorithm distributes the adjustment uniformly across all trainable parameters, thereby preventing instability in the parameter updates. Effectively, this approach allowed the optimization process to interpolate between the Gauss–Newton method and gradient descent, adapting the step size and direction based on the local curvature of the loss landscape. Such an adaptive mechanism enhanced both the convergence rate and robustness of the training procedure. Consequently, the update of network parameters under the LM algorithm can be expressed as follows:

$$w^{(i+1)} = w^{(i)} - (J^{(i)T}.J^{(i)} + \lambda^{(i)} I)^{-1}(2J^{(i)T}.e^{(i)}) \tag{9}$$

3.2.MSE

MSE was widely used to assess the performance of regression models. It basically measured the average squared difference between predicted and observed values, giving you a sense of prediction precision. At first, the deviation of each prediction from its real value was computed; these deviations were then squared, which removed the negative sign and made larger deviations stand out more. After that, the sum of those squared deviations was divided by the total number of observations to produce the MSE. Because MSE amplifies larger errors by squaring, a model whose predictions wander far from actual values tends to have a higher MSE; conversely, a lower MSE indicates a model with higher predictive accuracy and better alignment with observed data. This metric was therefore valuable not only for evaluating a model's overall accuracy but also for assessing its sensitivity and robustness to data variations.

$$MSE = \frac{\sum_{i=1}^{n}(Y_i - \hat{Y}_i)^2}{n} \tag{10}$$

In Eq. 10, Yi represents the actual measured value for i-th observation, while n denotes the total number of data points included in the analysis. The corresponding $\hat{Y}_i$ value refers to the prediction made by the ANN for the same observation. This model aimed to minimize the discrepancies between predicted and actual values for all data points in the dataset. The extent of these differences provided a quantitative measure of ANN's accuracy, reflecting how closely it can replicate the actual outcomes.

4. Prediction Results and Analysis

4.1. K-fold Cross-Validation

To comprehensively assess the predictive capability and generalization performance of the developed ANN models, K-fold cross-validation was used. This resampling-based validation strategy was recognized as one of the most reliable approaches for maximizing data utilization while providing an unbiased assessment of the model performance on unseen data. In this method, the entire dataset was randomly divided into k approximately equal subsets (folds), allowing all data samples to participate in both the training and validation stages throughout the validation process. Such a strategy minimized the dependence of model evaluation on a specific train–test partition and improved the robustness of the results. During each iteration of the K-fold cross-validation procedure, k−1 folds were combined and used for network training, while the remaining fold was employed as an independent validation dataset for performance assessment. This process was repeated k times so that each fold was used exactly once as the validation set. The final predictive function of the ANN model was then determined by averaging the statistical performance metrics over all validation cycles. Compared with a single train–test split, this approach provided a more reliable estimate of the predictive accuracy and stability of the developed model. Furthermore, K-fold cross-validation enabled the identification of potential overfitting or underfitting by analyzing performance variations across folds. To further assess the robustness and reliability of the proposed ANN architecture, the CV of errors was calculated for each fold during the k=5 cross-validation process. The CV parameter was defined as the ratio of the standard deviation of the prediction errors for the test samples to the mean of the associated target outputs. The obtained CV values for predicting the Max plate stress varied from 0.0885 to 0.0947, all of which remained below the stability threshold of 0.10. These results confirmed the stable predictive performance of the developed ANN model and indicated the absence of significant overfitting during training.

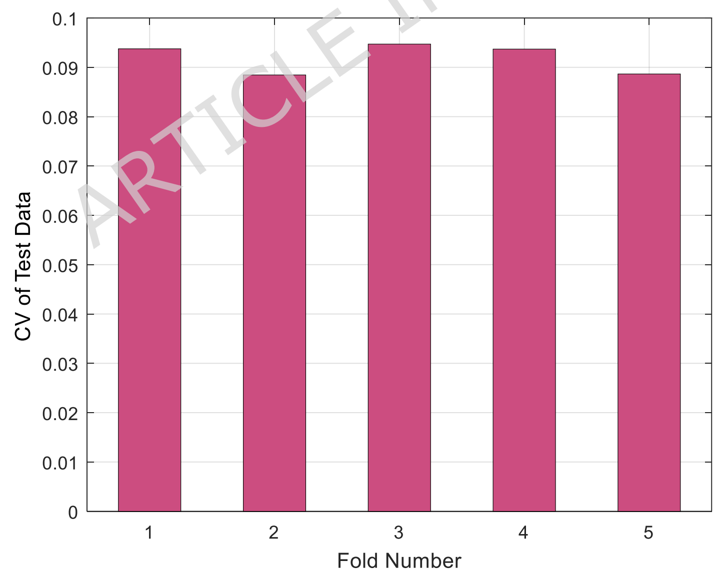

Fig.7: CV of test data corresponding to 5 partitions made by the K-fold Cross Validation approach

Fig. 8 presents the CV for the thermal conductivity test data obtained from the 10 partitions generated by the K-fold cross-validation procedure. CV values showed noticeable variations across folds, indicating differences in the statistical distributions and prediction complexities of the individual test subsets. However, all calculated CV values remained below the stability threshold of 0.10, confirming the stable and reliable predictive performance of the developed ANN model. Furthermore, the relatively low CV values across several folds demonstrate strong predictive consistency and satisfactory generalization capability of the network, while the absence of excessive fluctuations indicates that significant overfitting did not occur during training.

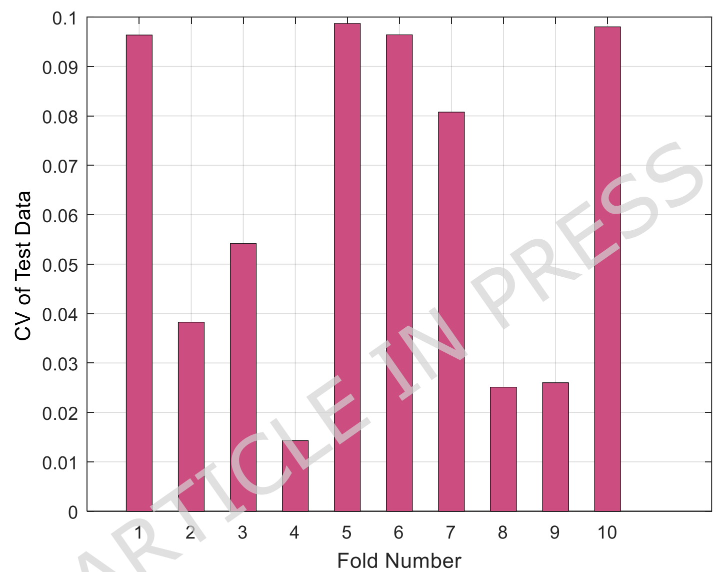

Fig.8: CV of thermal conductivity test data corresponding to 10 partitions made by the K-fold Cross Validation approach.

4.2.Comparison of different performance functions

The corresponding performance plot for the ANN developed to predict the Maximum stress of a laminated composite plate is shown in Fig. 9. The overall decreasing trend in MSE was clearly observable across the training, validation, and test data subsets until the network achieved its optimal performance. The point corresponding to the Minimum validation error, marked with a green circle in the figure, represents the most accurate stage of network training. In this case, the best validation performance was achieved at epoch 22, with an MSE value of 3.2266×10^{-4}.

Additionally, the Min MSE attained for the entire dataset using the ANN was 6.5566×10^{-4}. The observed downward trend in MSE not only confirmed the proper convergence of the training algorithm but also showed the ANN's strong ability to generalize input–output relationships.

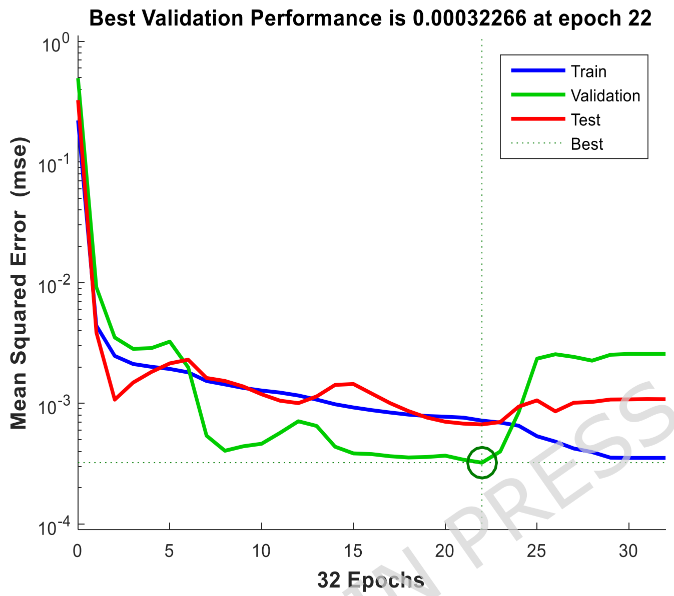

Fig. 9: ANN function graph via the optimization steps of the corresponding MSE index for every set of training, validation, and testing data.

Another important criterion for evaluating the quality of ANN training was the regression plots and the corresponding correlation coefficients (R) between the predicted outputs and the target values. These results for the trained network are illustrated in Fig. 10. In this Fig, the final ANN outputs for each data subset (training, validation, and testing) were plotted on the vertical axis against the target values obtained from the FE model on the horizontal axis. Ideally, a perfectly trained network should yield outputs identical to the targets, corresponding to an MSE of zero. In such a case, the R would equal 1, the slope of the regression line would be 1, and the intercept (bias) would be zero. The results shown in Fig. 10 indicate that the ANN outputs closely match the target values across all datasets. The R for the training, validation, testing, and overall datasets were 0.99508, 0.98649, 0.99484, and 0.99485, respectively. All of these values were very close to the ideal value of 1. This demonstrated that the designed ANN had excellent predictive capability and could accurately estimate the maximum stress of the composite plate across fiber orientations from 0° to 90°.

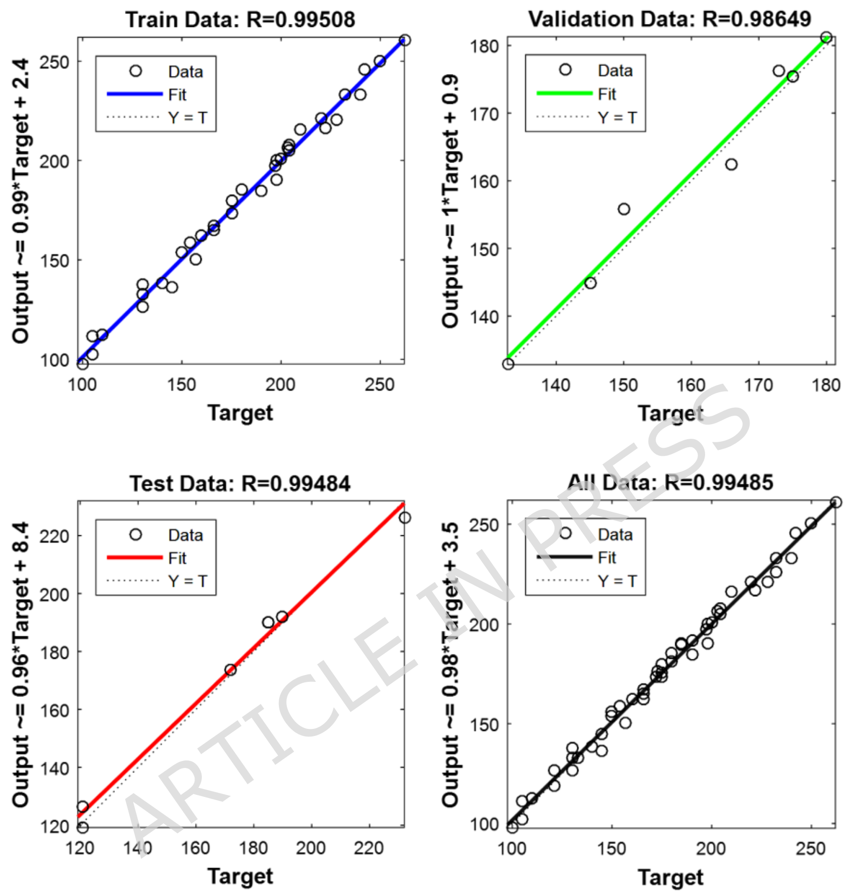

Fig.**10:** ANN regression plot corresponding to each set of training, validation, and testing data and the total data.

The fitted curves and the corresponding relative error percentages for the trained ANN are presented in Fig. 11 for the test dataset. The relative error percentage was defined as the ratio of the difference between the actual values obtained from the FE model and the ANN's predicted outputs to the exact values. The results reveal very close agreement between the expected outputs and the target values, with relative errors in the test data negligibly small. This strong consistency demonstrated both the reliability and the accuracy of the trained network. Further quantitative analysis indicated that the average and Max relative errors for the testing dataset were 2.2497% and 4.4122**%**, respectively. These low error values confirmed the high precision of the designed ANN in estimating the maximum stress of the composite plate across a wide range of fiber orientation angles in the two-layer configuration. Overall, the results demonstrated the robust predictive performance of the proposed model, even when applied to previously unseen data, and confirm its ability to capture the stress response of composite plate studied accurately.

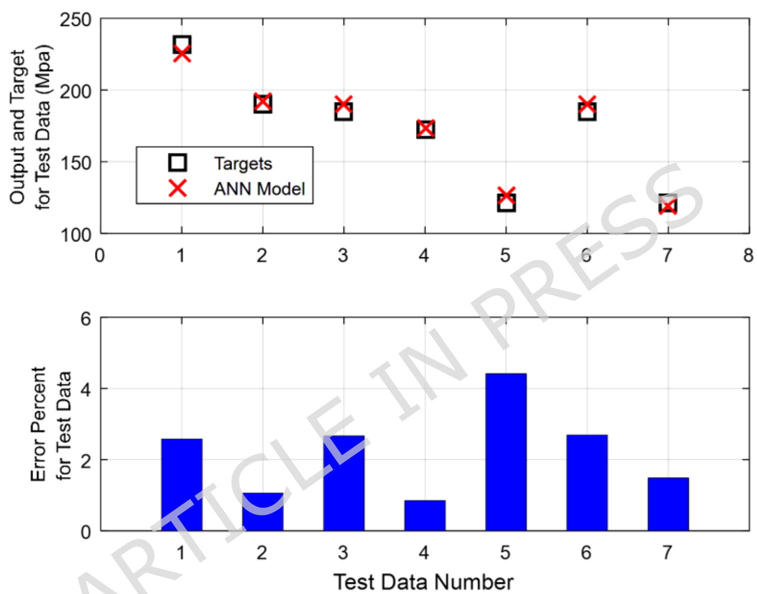

Fig.11: Adaptation plots and percentage error of sheet stress values compared to ANN outputs, for test data.

Moreover, the data points in Fig. 12 depict the absolute errors between the ANN-predicted outputs and the corresponding actual values obtained from the FE model. These errors were presented as a function of the fiber orientation angles in both layers of the composite. Analysis of the results indicated that Min, Max, and average predicted Max stresses were 0.0109, 8.6430, and 3.4170 MPa, respectively. The negligible magnitude of these errors clearly demonstrated the ANN model's excellent predictive capability. Overall, these findings confirmed that the trained network can accurately capture the stress distribution in the composite plate across a wide range of fiber orientations, demonstrating the robustness and generalization of the proposed approach.

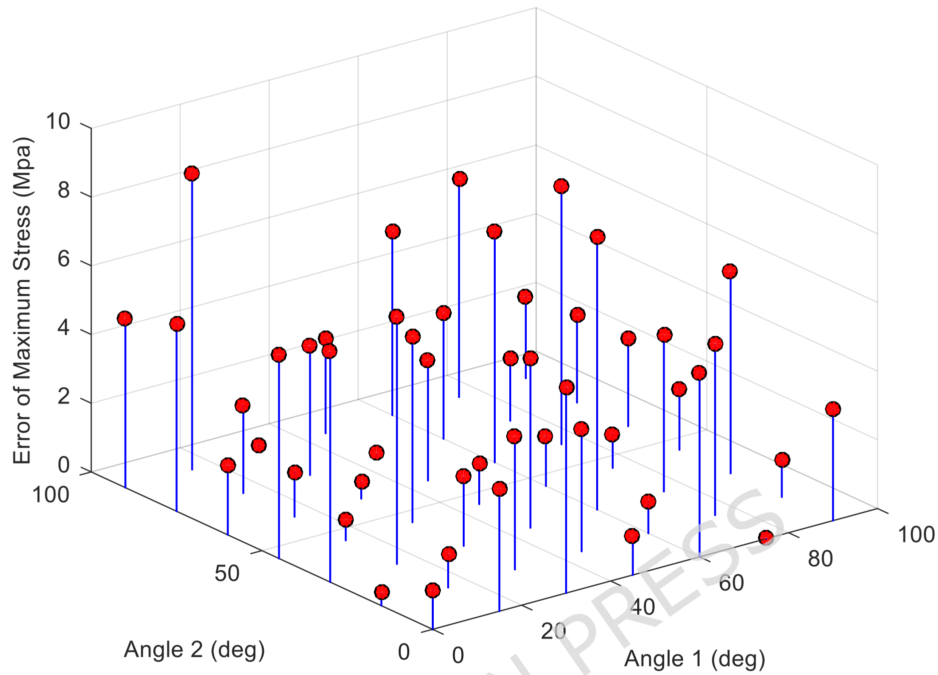

Fig.12: Absolute values of the error in estimating the maximum stress of the composite sheet in terms of the angles of the two-layer fibers for all data obtained from the FE model.

The continuous response surface of the trained ANN model's outputs is illustrated in Fig. 13 as a function of constant variations in the fiber orientation angles of two composite layers. Individual red star markers indicated the actual stress values obtained from the FE model for the training dataset. These points aligned closely with the ANN-predicted response surface, confirming the network's accuracy in reproducing the training data. The response surface showed a smooth topology, with no sharp peaks or pronounced irregularities. This smoothness, together with the proximity of data points to the predicted surface and the stress variation trends observed in Fig. 3, provides strong evidence that the network did not overfit during training. These results indicate that the trained ANN model can reliably predict the composite plate's maximum stress for arbitrary fiber orientation angles within the defined input range. The smooth, continuous nature of the response surface further demonstrated the network's robustness and generalization capability, confirming its applicability for accurate stress estimation in the two-layer composite configuration.

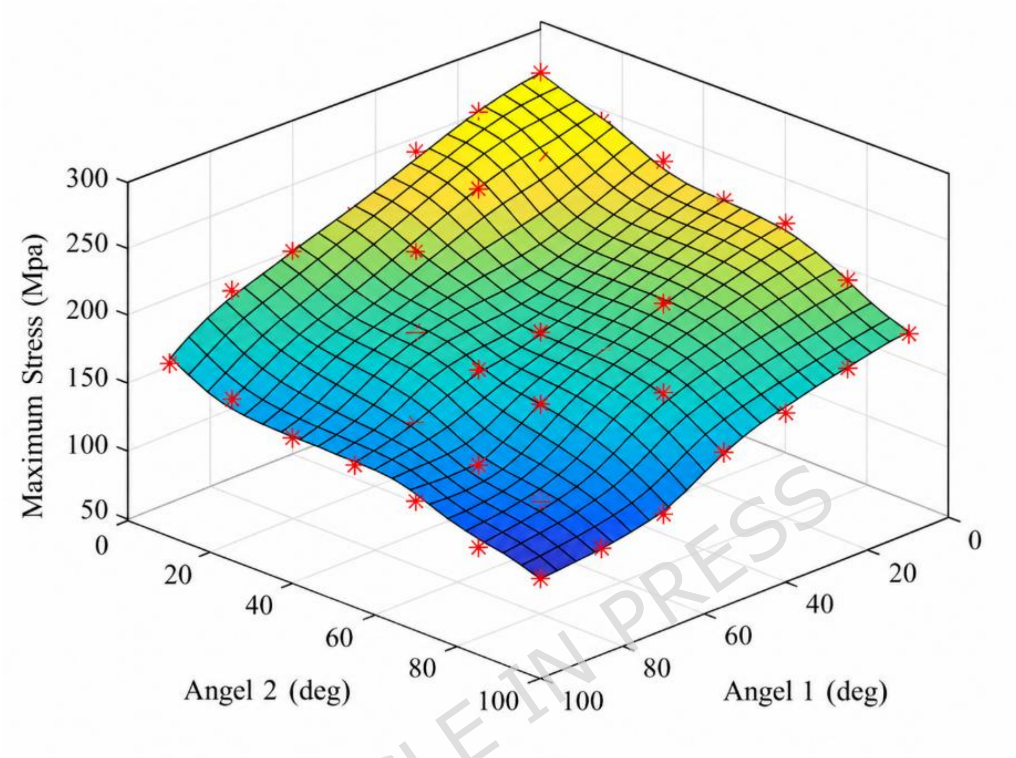

Fig.13: Response curve of the Max stress output of the composite sheet in terms of the two-layer fiber angles, along with points corresponding to the actual values obtained from the FE model for all data.

5. Variance-Based Global Sensitivity Analysis Using the Sobol Method

To quantitatively assess the relative influence of input parameters on the ANN model's predicted output responses, a variance-based Global Sensitivity Analysis (GSA) was performed using the Sobol method. Among existing sensitivity analysis techniques, the Sobol approach is recognized as one of the most rigorous and reliable methods for nonlinear and non-monotonic systems because it enables the complete decomposition of output variance into contributions from individual input variables and their mutual interactions [25]. Considering a general mathematical model expressed as:

$$Y = f = (X_1, X_2, \ldots, X_k) \tag{11}$$

where Y denotes the model response and X_i (i=1,2,…,k) represent independent input variables, the Sobol method is based on the functional Analysis of Variance (ANOVA) decomposition of the model function. Accordingly, the model can be decomposed as follows [25]:

$$f(X) = f_0 + \sum_{i-1}^{k} f_i(X_i) + \sum_{i<j} f_{ij}(X_i, X_j) + \ldots + f_{12\ldots k}(X_1, X_2 \ldots, X_k) \tag{12}$$

where f_0 is a constant term corresponding to the expected value of the model output, fi(Xi) represents the first-order effect of variable X_i, and $f_{ij}(X_i, X_j)$ denotes the interaction effect between variables X_i and X_j. Higher-order terms represent simultaneous interactions among multiple variables. Assuming statistical independence among the input variables, the total variance of the model response can be decomposed into additive variance contributions as [25]:

$$Var(Y) = \sum_{i=1}^{k} V_i + \sum_{i<j} V_{ij} + \ldots + V_{12\ldots k} \tag{13}$$

where:

$$V_i = Var[E(Y \mid X_i)] \tag{14}$$

is the first-order variance contribution associated with variable X_i, while V_{ij} represents the second-order interaction variance contribution between X_i and X_j. Based on these variance components, Sobol sensitivity indices can be defined to quantify the contribution of each variable and its interactions to the total output uncertainty. The first-order Sobol index is expressed as:

$$S_i = \frac{V_i}{Var(Y)} \tag{15}$$

which measures the direct contribution of the input variable X_i to the output variance. The second-order interaction index is given by:

$$S_{ij} = \frac{V_{ij}}{Var(Y)} \quad (16)$$

which quantifies the interaction effect between variables X_i and X_j. In addition, the total-order Sobol index is defined as [26, 27]:

$$ST_i = 1 - \frac{Var[E(Y|X_{\sim i})]}{Var(Y)} \quad (17)$$

where X~i represents the set of all variables except X_i. The total-order index reflects Xi's overall contribution, including both its direct effect and all higher-order interactions involving Xi. The interpretation of Sobol sensitivity indices provided valuable insight into the system's governing behavior. A large value of S_i indicates that the corresponding variable had a strong direct influence on the model response. Conversely, a large difference between ST_i and S_i indicated that the variable significantly interacts with other variables.

Furthermore, when the summation of first-order indices approaches unity ($\sum S_i \approx 1$), interaction effects were considered negligible, whereas significantly higher-order indices indicated nonlinear coupling behavior among the input variables. In practical applications, Sobol sensitivity indices were typically estimated using Monte Carlo or quasi-random sampling methods. In the present study, a nonlinear ANN model was developed to predict the maximum stress of a two-layer composite plate based on the fiber orientation angles of the two layers. Due to the ANN's nonlinear, data-driven nature, a variance-based Global Sensitivity Analysis (GSA) using the Sobol method was performed to quantitatively evaluate the relative influence of input variables on the predicted response. Sobol analysis was carried out using 10,000 base samples generated through the Saltelli sampling scheme, which was widely recognized for improving the computational efficiency and accuracy of variance estimation in high-dimensional nonlinear models [26, 27]. Accordingly, the first-order (S_1), total-order (S_T), and second-order interaction (S_{12}) sensitivity indices were calculated. Table 4 presents the calculated first- and total-order Sobol sensitivity indices for the fiber orientation angles of two composite layers. The results indicated that both input variables exerted a significant influence on the variance of the predicted Max stress. A notable observation was the numerical difference among the sensitivity indices associated with the first-layer and second-layer fiber angles. Specifically, the second-layer fiber angle exhibited a higher total-order sensitivity index (S_T=0.679) compared with the first-layer fiber angle (S_T=0.328). From a theoretical perspective, assuming perfectly symmetric geometry and loading conditions, identical sensitivity contributions would generally be expected for both variables. However, such numerical asymmetry was a known characteristic in surrogate and meta-modeling approaches based on ANN architectures. This discrepancy can be attributed to the stochastic nature of the ANN training process and the random distribution of weights and biases within the hidden layers, which may slightly amplify the sensitivity of one input variable over another within the feature space representation. In general, ANN models function as statistical approximators, and achieving perfect mathematical symmetry requires infinitely large datasets and fully symmetric training conditions, which are rarely attainable in practical engineering applications. Furthermore, the relatively small value of the second-order interaction index (S_{12}=0.008) indicated that the direct interaction between the two fiber orientation angles is weak. This observation confirmed that the fiber orientation angle of each layer independently contributed to the distribution of predicted maximum stress within the developed ANN model.

Table 4: The direct and interaction contribution of two input variables of fiber angles of layers to the variance of the maximum stress as output

Parameter	S1 (First Order)	ST (Total Order)
Angle 1	0.319	0.328
Angle 2	0.673	0.679

Fig.14 further illustrates the response surface generated by the developed ANN model for changes in the fiber orientation angles of the first and second composite layers within the range of 0∘to 90∘. The colored contour distributions show an overall decrease in the predicted maximum stress with increasing fiber orientation angle, with minimum stress values observed in the high-angle region near 90∘. This behavior was consistent with the expected stress redistribution mechanism in laminated composite structures and demonstrated the influence of fiber orientation on the load-transfer characteristics of the composite plate. A detailed examination of contour symmetry with respect to the diagonal bisector line revealed slight local deviations and minor waviness in some intermediate regions of the response surface. In addition to the inherent nonlinear behavior of the ANN model, these numerical asymmetries may also arise from computational artifacts in the FE analysis dataset used for ANN training. Since the ANN model was trained on 49 numerical samples, local sensitivities at the sampling points can influence the formation of contour curvatures, particularly in transitional regions of the design space. Nevertheless, the overall response trend and the global stress variation gradients across the entire parameter domain remained physically consistent with the established principles of composite mechanics. The developed ANN model successfully identified both critical and optimal regions within the design space, thereby demonstrating its reliability and robustness in approximating the complex nonlinear physics governing the mechanical behavior of laminated composite structures.

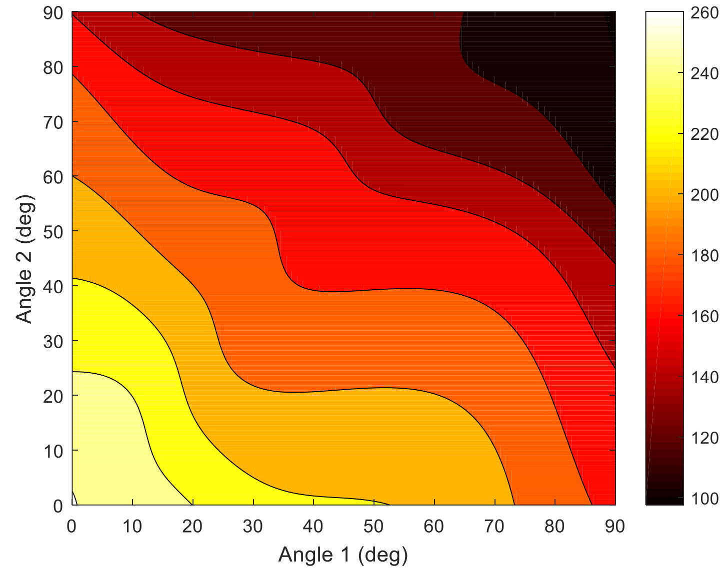

Fig.14. Color contour of the response surface of the Max stress of a two-layer composite sheet in terms of two variables: the fiber angles of the layers.

6. Conclusion

In this study, a computational FE-ANN framework was developed to forecast the corrected Maximum stress behavior of laminated composite plates subjected to fully reversed cyclic loading. FE simulations based on the Morrow-corrected stress analysis were performed for various combinations of fiber orientation angles, and the resulting numerical dataset was used to train a single-hidden-layer feedforward ANN. The developed framework provides a computationally efficient alternative to repeated FE simulations for stress-based fatigue assessment of laminated composite structures. The principal results of the present study can be summarized as follows:

- The developed ANN model demonstrated strong predictive capability and generalization, achieving an optimal validation MSE of 3.2266×10^{-4} and overall regression coefficients exceeding 0.98 across all datasets.
- K-fold cross-validation confirmed the robustness and stability of the proposed ANN architecture, with CV values ranging from 0.0885 to 0.0947, all of which remained below

the stability threshold of 0.10, indicating the absence of significant overfitting.

- Fiber orientation strongly influenced the corrected Max stress distribution within the laminated composite plate. Increasing the fiber orientation angles generally reduced the predicted stress levels, while Min stress values were observed near the 90° fiber orientation configuration.
- Variance-based Sobol sensitivity analysis revealed that the second-layer fiber orientation angle exerted a stronger influence on the predicted Max stress than the first-layer orientation angle, while the interaction effects between the two variables remained relatively weak.
- The ANN-generated response surfaces and stress contour analyses successfully identified critical stress-concentration regions and stress-sensitive fiber-orientation configurations within the investigated design domain.
- The proposed FE-ANN framework demonstrated reliable capability for rapid stress estimation and fatigue-related stress assessment in laminated composite structures, significantly reducing the computational cost associated with repeated FE simulations.

Overall, the obtained results confirm that ANN-based surrogate modeling can provide an effective and reliable computational tool for nonlinear stress prediction and preliminary fatigue-sensitive assessment of composite laminates under cyclic loading conditions.

6.1. Limitations and Future Work

Although the present study primarily focused on predicting the corrected Max stress response rather than directly estimating fatigue life, the obtained stress distributions provided valuable insight into fatigue-sensitive regions and potential crack-initiation zones within the laminated composite structure. Since fatigue damage initiation in composite materials was strongly associated with local stress concentration and cyclic stress redistribution, the developed FE-ANN framework can serve as an efficient preliminary assessment tool for identifying critical fiber orientation configurations before more computationally intensive fatigue-life analyses. In addition, the present FE framework did not include explicit progressive damage evolution mechanisms such as stiffness degradation, delamination growth, matrix cracking, or continuum damage mechanics formulations. Therefore, the current model should be interpreted as a stress-based fatigue assessment methodology rather than a complete fatigue-life prediction framework. Future investigations may extend the proposed methodology toward direct fatigue-life estimation and progressive damage prediction using experimentally validated fatigue criteria, multiscale damage evolution models, and larger training datasets for advanced ANN-based surrogate modeling.

Declaration

Ethics approval and consent to participate: Not Applicable

- **Consent for publication:** Not Applicable
- **Competing interests:** Not Applicable

- **Authors' contributions:** Not Applicable
- **Acknowledgments:** Not Applicable
- **Availability of data and material:** Not Applicable

Data Availability Statement

The data that support the findings of this study are available from the corresponding author, upon reasonable request.

Funding Declaration: Not Applicable

References

[1] K. K. Chawla, *Composite materials: science and engineering*. Springer Science & Business Media, 2012.

[2] M. K. Egbo, "A fundamental review on composite materials and some of their applications in biomedical engineering," *Journal of King Saud University-Engineering Sciences,* vol. 33, no. 8, pp. 557-568, 2021.

[3] D. K. Rajak, D. D. Pagar, R. Kumar, and C. I. Pruncu, "Recent progress of reinforcement materials: a comprehensive overview of composite materials," *Journal of Materials Research and Technology,* vol. 8, no. 6, pp. 6354-6374, 2019.

[4] S. S. Sorour, C. A. Saleh, and M. Shazly, "A review on machine learning implementation for predicting and optimizing the mechanical behaviour of laminated fiber-reinforced polymer composites," *Heliyon,* vol. 10, no. 13, 2024.

[5] A. Memarzadeh, E. C. Onyibo, M. Asmael, and B. Safaei, "Dynamic effect of ply angle and fiber orientation on composite plates," *Spectrum of Mechanical Engineering and Operational Research,* vol. 1, no. 1, pp. 90-110, 2024.

[6] Z. Lei, R. Pan, W. Sun, Y. Dong, Y. Wan, and B. Yin, "Fatigue damage mechanisms and evolution of residual tensile strength in CFRP Composites: stacking sequence effect," *Composite Structures,* vol. 330, p. 117818, 2024.

[7] A. Mahmoudi, B. Mohammadi, and H. Hosseini-Toudeshky, "Damage behaviour of laminated composites during fatigue loading," *Fatigue & Fracture of Engineering Materials & Structures,* vol. 43, no. 4, pp. 698-710, 2020.

[8] A. Gupta and M. Singh, "Comparative study of failure analysis in glass fiber reinforced laminated pin joints under cyclic and static loading conditions," *Journal of Composite Materials,* vol. 58, no. 5, pp. 661-675, 2024.

[9] J. Thomas, A. Davis, and M. P. Samuel, "Quality-reliability-risk-safety paradigm—analyzing fatigue failure of aeronautical components in light of system safety principles," in *Fatigue, Durability, and Fracture Mechanics: Proceedings of Fatigue Durability India 2019*: Springer, 2020, pp. 267-304.

[10] A. Ince, "A mean stress correction model for tensile and compressive mean stress fatigue loadings," *Fatigue & Fracture of Engineering Materials & Structures,* vol. 40, no. 6, pp. 939-948, 2017.

[11] A. Niesłony and M. Böhm, "Universal method for applying the mean-stress effect correction in stochastic fatigue-damage accumulation," *Materials Performance and Characterization,* vol. 5, no. 3, pp. 352-363, 2016.

[12] G. Wei, Z. Hao, G. Chen, H. Ke, L. Deng, and L. Liu, "Rapid assessment of out-of-plane nonlinear shear stress–strain response for thick-section composites using artificial neural networks and DIC," *Composite Structures,* vol. 310, p. 116770, 2023.

[13] Y. Liu, H. A. Alkhazaleh, M. A. Khan, M. Samavatian, and V. Samavatian, "Local elasticity assessment of unidirectional fiber-reinforced polymer composites through impulse excitation and machine learning," *Journal of Reinforced Plastics and Composites,* p. 07316844241307083, 2024.

[14] E. Marković, T. Marohnić, and R. Basan, "A Surrogate Artificial Neural Network Model for Estimating the Fatigue Life of Steel Components Based on Finite Element Simulations," *Materials,* vol. 18, no. 12, p. 2756, 2025.

[15] A. Taherzadeh-Fard, A. Cornejo, S. Jiménez, and L. G. Barbu, "Numerical analysis of damage in composites: from intra-layer to delamination and data-assisted methods," *Mathematics,* vol. 13, no. 10, p. 1578, 2025.

[16] D. Samadian, I. B. Muhit, and N. Dawood, "Application of data-driven surrogate models in structural engineering: a literature review," *Archives of Computational Methods in Engineering,*

vol. 32, no. 2, pp. 735-784, 2025.
[17] W. Ramberg and W. R. Osgood, "Description of stress-strain curves by three parameters," 1943.
[18] N. A. Guerreiro, R. Nijo, and J. P. Teixeira, "Comparison of neural network architectures for diabetes prediction," *Procedia Computer Science*, vol. 256, pp. 942-948, 2025.
[19] Schmidhuber, J. (2015). Deep learning in neural networks: An overview. Neural Networks, 61, 85–117.
[20] J. A. Díaz-Sánchez, "Levenberg-Marquardt Algorithm," 2025.
[21] E. V. Castelani, E. Duran, R. Lopes, and A. E. Schwertner, "A Multi-step Algorithm Based on Levenberg-Marquardt Method for Solving LOVO Problems," in *Operations Research Forum*, 2025, vol. 6, no. 2: Springer, p. 45.
[22] A. Ranganathan, "The Levenberg-Marquardt algorithm," *Tutorial on LM algorithm,* vol. 11, no. 1, pp. 101-110, 2004.
[23] H. Yu and B. M. Wilamowski, "Levenberg–Marquardt training," in *Intelligent Systems*: CRC Press, 2018, pp. 12-1-12-16.
[24] M. I. Lourakis, "A brief description of the Levenberg-Marquardt algorithm implemented by levmar," *Foundation of Research and Technology,* vol. 4, no. 1, pp. 1-6, 2005.
[25] I. M. Sobol, "Sensitivity estimates for nonlinear mathematical models," *Math. Model. Comput. Exp.,* vol. 1, no. 4, pp. 407-414, 1993.
[26] A. Saltelli *et al.*, *Global sensitivity analysis: the primer*. John Wiley & Sons, 2008.
[27] A. Saltelli, P. Annoni, I. Azzini, F. Campolongo, M. Ratto, and S. Tarantola, "Variance based sensitivity analysis of model output. Design and estimator for the total sensitivity index," *Computer physics communications,* vol. 181, no. 2, pp. 259-270, 2010.

[27[Liu, H., Basem, A., Jasim, D. J., Hashemian, M., Ali Eftekhari, S., Al-fanhrawi, H. J., … Salahshour, S. (2025). Multi-objective optimization of buckling load and natural frequency in functionally graded porous nanobeams using non-dominated sorting genetic Algorithm-II. Engineering Applications of Artificial Intelligence, 142(109938), 109938. doi:10.1016/j.engappai.2024.109938

[28] Sharafati, A.; Haghbin, M.; Aldlemy, M.S.; Mussa, M.H.; Al Zand, A.W.; Ali, M.; Bhagat, S.K.; Al-Ansari, N.; Yaseen, Z.M. Development of Advanced Computer Aid Model for Shear Strength of Concrete Slender Beam Prediction. Appl. Sci. 2020, 10, 3811. https://doi.org/10.3390/app10113811

[29] Qader, D. N., Alzabeebee, S., Kandiri, A., Shakor, P., Saeed, S., & Al Hamd, R. K. S. (2026). Performance analysis of concrete-filled aluminum tubes confined with aramid fiber sheets under axial loading: a combined numerical and machine learning approach. Multiscale and Multidisciplinary Modeling Experiments and Design, 9(1). doi:10.1007/s41939-025-01082-w